LIMNOLOGY AND OCEANOGRAPHY
Letters

ASLO
Open Access

Limnology and Oceanography Letters 3, 2018, 265–274

doi: 10.1002/lol2.10062

SPECIAL ISSUE-LETTER

Velocity-amplified microbial respiration rates in the lower Amazon River

Nicholas D. Ward [1,2,3]* *Henrique O. Sawakuchi,*[2,4] *Vania Neu,*[5] *Diani F. S. Less,*[6] *Aline M. Valerio,*[7] *Alan C. Cunha* [6] *Milton Kampel,*[7] *Thomas S. Bianchi,*[3] *Alex V. Krusche,*[4] *Jeffrey E. Richey,*[2] *Richard G. Keil*[2]

[1]Marine Sciences Laboratory, Pacific Northwest National Laboratory, Sequim, Washington; [2]School of Oceanography, University of Washington, Seattle, Washington; [3]Department of Geological Sciences, University of Florida, Gainesville, Florida; [4]Centro de Energia Nuclear na Agricultura, Universidade de São Paulo, Piracicaba, São Paulo, Brazil; [5]Instituto Socio Ambiental e dos Recursos Hidricos, Universidade Federal Rural da Amazonia, Belem, Pará, Brazil; [6]Departamento de Meio Ambiente e Desenvolvimento, Universidade Federal do Amapá, Macapá, Amapá, Brazil; [7]Divisão de Sensoriamento Remoto, Instituto Nacional de Pesquisas Espaciais, São José dos Campos, São Paulo, Brazil

Scientific Significance Statement

Most measurements of aquatic respiration in large rivers ignore the influence of river flow on reaction rates, which we hypothesize has resulted in an underestimation of the contribution of microbial respiration to CO_2 outgassing in large tropical rivers. Here, we evaluate microbial respiration rates along the lower Amazon River under different simulated flow conditions using rotating incubation chambers. We demonstrated that river velocity and hydrodynamic conditions are key factors controlling microbial metabolism of river-borne organic matter, and that microbial respiration can potentially exceed CO_2 outgassing rates in the Amazon River mainstem and be balanced by primary production, outgassing, and other inputs.

Abstract

Most measurements of respiration rates in large tropical rivers do not account for the influence of river flow conditions on microbial activity. We developed a ship-board spinning incubation system for measuring O_2 drawdown under different rotation velocities and deployed the system along the lower Amazon River during four hydrologic periods. Average respiration rates in incubation chambers rotated at 0.22 m s^{-1} and 0.66 m s^{-1} were 1.4 and 2.4 times higher than stationary chambers, respectively. On average, depth-integrated

*Correspondence: nicholas.ward@pnnl.gov

Author Contribution Statement: RGK conceived the idea for continuous O_2 monitoring in a closed chamber, originally designed for use in the ocean. NDW and AVK adapted the design to replicate rapidly mixed river waters. NDW and HOS performed lab tests and field deployment of the incubation system with the assistance of VN, AMV, DFSL, MK, and TSB. Traditional BOD respiration experiments were performed by DFSL under the supervision of NDW, VN, and AVK. Field sampling logistics were overseen and coordinated by AVK, JER, HOS, and NDW and organized locally by ACC. The experimental ideology was conceived by RGK and NDW. The manuscript was prepared by NDW and discussed/commented on between all authors.

Data Availability Statement: Data are available in the Figshare repository at https://figshare.com/collections/Ward_et_al_Limnology_and_Oceanography_Letters_2018_/3966822.

Additional Supporting Information may be found in the online version of this article.

This article is part of the Special Issue: Carbon cycling in inland waters
Edited by: Emily Stanley and Paul del Giorgio

respiration rates in chambers spun at 0.22 m s^{-1} and 0.66 m s^{-1} accounted for 64% ± 22% and 104% ± 36% of CO_2 outgassing rates, respectively, in mainstem sites. Continuous measurements of in situ pCO_2 were also made along with cross-channel profiles of river velocity. A positive correlation between river velocity and pCO_2 was observed along the lower river ($r^2 = 0.67$–0.96) and throughout a tidal cycle.

The complex consortium of organic substrates and microorganisms in inland aquatic ecosystems yield high rates of biological respiration relative to marine systems (del Giorgio and Williams 2005). As such, inland waters serve as bioreactors that efficiently transform organic substrates derived from terrestrial and aquatic primary production into carbon dioxide (CO_2), fueling CO_2 evasion from the world's rivers and lakes along with lateral inputs (Tranvik et al. 2009; Ward et al. 2017). In large tropical river systems, which, along with their floodplains, contribute disproportionately to global inland water CO_2 emissions (Aufdenkampe et al. 2011; Raymond et al. 2013), heterotrophic respiration is often considered to be the primary mechanism for aquatic CO_2 super saturation in the river mainstem (Mayorga et al. 2005; Ward et al. 2013). However, in the few circumstances that CO_2 outgassing and respiration rates were measured simultaneously in the world's largest river, the Amazon River, depth-integrated respiration rates could only account for 29% ± 32% of CO_2 outgassing in the mainstem and less than 1% in some tributaries (Ellis et al. 2012).

The mismatch between respiration and CO_2 outgassing rates is typically attributed to a combination of influence from of other CO_2 sources to the river such as floodplains (Abril et al. 2014; Melack 2016), the soil–water interface (McClain et al. 2003), and small streams (Johnson et al. 2008). While not discounting these inputs, we hypothesize that incubation-based respiration rates in the Amazon River mainstem have been underestimated.

Resolving the contribution of organic matter (OM) decomposition to regional carbon balances is essential for predicting the response of aquatic systems to future change and requires identification of the biases associated with analytical protocols. Aquatic respiration rates in the Amazon River have been determined by measuring O_2 drawdown during dark incubations in small bottles that are shaken periodically (Benner et al. 1995; Ellis et al. 2012; Ward et al. 2013). In less remote systems, the state of the art for modeling ecosystem respiration is based on measurements of in situ conditions such as the concentration and stable isotopic composition of dissolved O_2 (Hotchkiss and Hall 2014) or site-specific pCO_2 and net ecosystem productivity (Marcarelli et al. 2011; Hotchkiss et al. 2015). However, these techniques are not logistically feasible in the Amazon River, where current velocities can exceed 1.8 m s^{-1}, depths can reach nearly 100 m (average cross channel depths ranged from 15.4 m to 51.5 m in this study; Table 1), bank erosion can dislodge trees that one might attach instrumentation to, and an active shipping channel prevents mooring placement.

For this reason, we developed a ship-board rotating incubation system (Supporting Information Fig. S1) that allows samples to be disturbed at variable speeds, which we hypothesize reflects the mixing conditions (i.e., ability to maintain particles in suspension) associated with different river flow velocities based on insight from fluid dynamics experiments (e.g., Ivanova et al. 2004). This system provides data in real-time allowing for adaptability in the field and observations of temporally variable O_2 drawdown rates throughout the incubation. Respiration experiments were performed using traditional methods (Benner et al. 1995) and this new system along the lower Amazon River (Fig. 1). CO_2 outgassing rates were simultaneously measured in floating chambers (Sawakuchi et al. 2017) to evaluate the contribution of depth-integrated respiration to CO_2 evasion. While there are uncertainties associated with floating chambers (Kremer et al. 2003; Matthews et al. 2003), we have chosen a similar approach used by Ellis et al. (2012) for consistency, and when properly designed and managed, floating chambers are a cost-effective way of obtaining site-specific gas transfer velocities for specific environments, as opposed to using models developed for other systems (Cole et al. 2010; Gålfalk et al. 2013; Lorke et al. 2015). pCO_2 was also measured throughout the sampling campaign and river velocity was measured across each sampling station using an acoustic Doppler current profiler (ADCP). We hypothesize that respiration rates respond to flow regime in relation to the extent of particle suspension, which results in a positive relationship between pCO_2 and river velocity.

Methods

Four expeditions were performed along the lower Amazon River from April 2014 to March 2016 during low, rising, high, and falling river discharge periods (Fig. 1). The study domain spanned from Óbidos to the last two well-constrained channels near Macapá (Fig. 1). The region from Óbidos to the river mouth encompasses roughly 13% of the basin's total surface area of 5.83×10^6 km^2. This region is characterized by expansive floodplains, covering about 17% of the lower Amazon basin (Hess et al. 2015), and a main river channel that becomes wider and slower toward the mouth, covering ~ 1.3% of the lower basin's surface area (Sawakuchi et al. 2017). The effects of tides dampen river flow even upstream of Almeirim and reverse the river's flow near the mouth during peak rising tide (Ward et al. 2015). The clear waters of the Tapajós and Xingu Rivers downstream of Óbidos are in contrast to the turbid

Table 1. River depth, velocity, discharge, Reynold's number (Re), CO_2 outgassing rates (Sawakuchi et al. 2017), and depth-integrated respiration rates measured in BOD bottles, in stationary incubation chambers (R_{STAT}), and chambers spinning at 0.22 m s^{-1} (R_{1x}) and 0.66 m s^{-1} (R_{3x}).

Station/date	Depth (m)	Velocity (m s^{-1})	Discharge (m^3 s^{-1})	Re	R_{BOD}* (g C m^{-2} d^{-1})	R_{STAT}* (g C m^{-2} d^{-1})	R_{1x}* (g C m^{-2} d^{-1})	R_{3x}* (g C m^{-2} d^{-1})	CO_2 outgassing (g m^{-2} d^{-1})
Obidos									
01 May 2014	54.7	1.66	253,879	1.1E+08	—	—	—	—	—
06 Nov 2014	51.1	1.01	122,274	6.2E+07	2.2 ± 0.5	—	7.8 ± 0.5	—	12.2 ± 4.2
04 Jul 2015	54.0	1.76	257,277	1.1E+08	3.5 ± 1.2	3.6 ± 0.8	6.7 ± 0.1	12.3 ± 1.5	20.5 ± 7.4
21 Feb 2016	49.3	0.99	122,172	5.9E+07	2.8 ± 0.9	7.2 ± 0.1	9.8 ± 1.6	16.9 ± 2.3	6.5 ± 2.9
Average	**51.5**	**1.36**	**167,241**	**8.6E+07**	**2.8 ± 0.7**	**5.4 ± 2.5**	**8.1 ± 1.6**	**14.6 ± 3.3**	**13.1 ± 7.0**
STM+50 km									
09 Nov 2014	38.5	0.95	126,389	4.5E+07	0.9 ± 0.0	—	—	—	—
09 Jul 2015	37.7	1.67	280,003	7.7E+07	3.0 ± 0.1	—	6.9 ± 0.3	12.1 ± 0.4	19.9 ± 2.3
24 Feb 2016	37.3	0.97	137,117	4.4E+07	1.7 ± 0.8	6.2 ± 0.2	8.8 ± 0.8	15.2 ± 0.3	4.1 ± 0.7
Average	**37.8**	**1.20**	**181,170**	**5.6E+07**	**1.9 ± 1.0**	**6.2 ± 0.2**	**7.9 ± 1.3**	**13.7 ± 2.2**	**12.0 ± 11.1**
Almeirim									
04 May 2014	29.0	1.51	298,913	5.4E+07	—	—	7.2 ± 0.1	—	15.7 ± 3.8
10 Nov 2014	26.2	0.75	124,831	2.4E+07	0.9 ± 0.3	—	5.6 ± 0.0	—	6.1 ± 1.9
11 Jul 2015	28.1	1.51	282,688	5.2E+07	1.4 ± 0.0	—	6.2 ± 0.2	8.6 ± 0.3	14.1 ± 4.8
25 Feb 2016	30.6	0.68	121,585	2.6E+07	1.4 ± 0.8	3.5 ± 0.1	5.9 ± 0.8	8.1 ± 0.8	2.6 ± 1.1
Average	**28.5**	**1.11**	**207,004**	**3.9E+07**	**1.2 ± 0.3**	**3.5 ± 0.1**	**6.2 ± 0.7**	**8.4 ± 0.4**	**9.6 ± 6.3**
North Macapa									
06 May 2014	18.7	0.75	140,624	1.8E+07	—	—	2.1 ± 0.0	—	17.4 ± 2.5
15 Nov 2014	19.0	0.53	61,539	1.2E+07	0.3 ± 0.1	—	4.5 ± 0.2	—	3.8 ± 0.6
16 Jul 2015	19.4	0.69	113,371	1.7E+07	0.7 ± 0.2	—	2.3 ± 0.0	4.8 ± 0.3	5.7 ± 2.8
03 Mar 2016	18.3	0.53	53,265	1.2E+07	0.7 ± 0.2	2.1 ± 0.1	2.6 ± 0.1	5.5 ± 0.2	2.2 ± 0.9
Average	**18.9**	**0.63**	**92,200**	**1.5E+07**	**0.6 ± 0.2**	**2.1 ± 0.1**	**2.9 ± 1.1**	**5.1 ± 0.5**	**7.3 ± 6.9**
South Macapa									
09 May 2014	24.1	0.75	204,056	2.2E+07	—	—	4.1 ± 0.1	—	17.9 ± 1.6
14 Nov 2014	23.6	0.61	132,998	1.8E+07	0.5 ± 0.3	—	5.0 ± 0.2	—	1.8 ± 0.1
14 Jul 2015	24.6	0.68	146,473	2.1E+07	1.1 ± 0.6	2.3 ± 0.1	4.6 ± 0.1	6.9 ± 0.1	4.1 ± 1.6
01 Mar 2016	24.3	0.59	103,593	1.8E+07	0.9 ± 0.1	3.8 ± 0.1	4.6 ± 0.7	6.2 ± 0.9	2.5 ± 1.0
Average	**24.1**	**0.66**	**146,780**	**2.0E+07**	**0.8 ± 0.3**	**3.0 ± 1.1**	**4.6 ± 0.4**	**6.5 ± 0.5**	**6.6 ± 7.6**
Tapajos River									
07 Nov 2016	24.0	0.09	3658	2.7E+06	1.1 ± 0.4	—	6.0 ± 0.4	—	0.8 ± 0.0
07 Jul 2015	23.5	0.20	10,018	5.8E+06	1.8 ± 0.8	3.6 ± 0.1	7.5 ± 0.2	12.8 ± 0.4	1.1 ± 0.3
22 Feb 2016	22.9	0.27	10,480	7.6E+06	2.0 ± 0.9	5.4 ± 0.3	6.4 ± 1.3	11.6 ± 0.8	2.5 ± 0.2
Average	**23.5**	**0.19**	**8052**	**5.4E+06**	**1.6 ± 0.5**	**4.5 ± 0.3**	**6.6 ± 0.7**	**12.2 ± 0.9**	**1.5 ± 0.9**
Xingu River									
06 May 2014	15.4	0.28	17,583	—	—	—	2.7 ± 0.1	—	8.1 ± 4.6
12 Nov 2016	15.4	0.03	1650	—	1.1 ± 0.7	—	5.0 ± 0.1	—	0.9 ± 0.4
12 Jul 2015	15.4	0.05	3200	—	1.6 ± 0.5	—	6.6 ± 0.3	8.9 ± 0.1	2.5 ± 1.0
27 Feb 2016	15.4	0.23	14,288	—	1.1 ± 0.1	2.8 ± 0.1	4.3 ± 0.6	6.4 ± 0.6	2.1 ± 0.3
Average	**15.4**	**0.15**	**9180**	—	**1.3 ± 0.3**	**2.8 ± 0.1**	**4.6 ± 1.6**	**7.7 ± 1.8**	**3.4 ± 3.2**

* Respiratation rates were determined based on a CO_2 production to O_2 drawdown ratio of 0.32 ± 0.08 for Amazon River mainstem sites and 0.46 ± 0.13 for the Tapajós and Xingu Rivers based on stable isotope probing experiments performed during the same study period (Ward et al. 2016).
—: Data required for calculations not available.

Amazon River waters and allow for high levels of primary production relative to the mainstem (Wissmar et al. 1981; Moreira-Turcq et al. 2003; Ward et al. 2016).

Dark incubation experiments were performed to determine the rate of biological oxygen consumption using three different techniques: (1) triplicate 60 mL biological oxygen

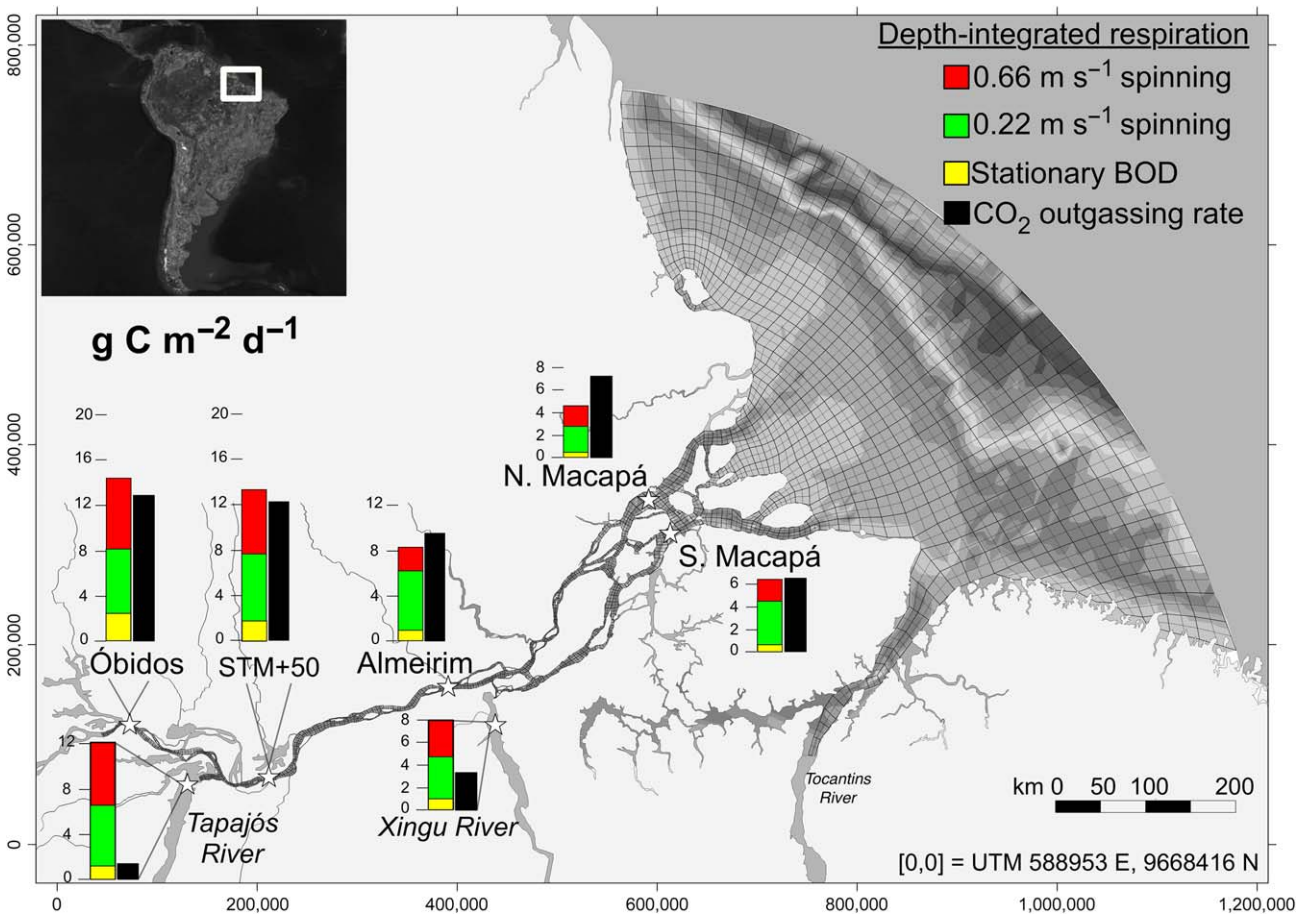

Fig. 1. Average CO_2 outgassing fluxes along the lower Amazon River (Sawakuchi et al. 2017) compared to depth-integrated respiration rates measured in stationary BOD bottles, incubation chambers spinning at 0.22 m s^{-1} and 0.66 m s^{-1}, and calculated velocity-normalized respiration rates based on measured river velocity and the correlation between chamber spin rate and observed respiration rates (g C m^{-2} d^{-1}).

demand (BOD) bottles with O_2 measured via Winkler titration (Benner et al. 1995; Ellis et al. 2012), (2) triplicate 60 mL BOD bottles with O_2 measured with a YSI ProODO optical probe, and (3) duplicate 2.85 L incubation chambers (48 cm height, 34 cm circumference) interfaced to YSI Exo 2 sonde optical dissolved O_2 probes (Supporting Information Figs. S1, S2).

For the 60 mL BOD incubations, dissolved O_2 was measured before and after a $\sim$ 24 h period. O_2 drawdown was assumed to be linear. Reported respiration rates represent the average measurement of the titration and optical probe methodologies and variability between the two methods were generally less than between replicates. In the 2.85 L chambers, dissolved O_2 measurements were logged on a 10–30 s interval throughout the incubation (Fig. 2). Chambers were affixed to Marconi spin plates and rotated at the minimum and maximum available speeds (20 rpm and 60 rpm, respectively), and an additional chamber was held stationary. The spin plate consists of a horizontally positioned central rotating axis, with attachment points for up to two of our custom chambers and one sonde that rotate around the axis (Supporting Information Fig. S1). O_2 sensors inserted inside the chambers prior to filling were attached to the sonde via custom cables. Blank tests were performed with the chambers using Milli-Q water, showing minimal variability (i.e., $\leq 1\%$) in dissolved O_2 concentrations (Supporting Information Fig. S3).

Chambers were filled with water from the center of each channel at 50% river depth using a Shurflo submersible pump typically during late morning hours. Fifty percentage depth was chosen as it reflects the average sediment distribution across the river's depth profile (Filizola and Guyot 2004). Chambers were overfilled for at least three times their volume without bubbling. Chambers were wrapped in reflective tape to exclude light and kept in the shade to maintain temperatures equivalent to river temperature (river and incubation chamber temperatures were within $\sim$ 1°C). Sixty milliliter BOD bottles were filled with water from 50% depth and the surface in triplicate at three stations located across the channel (left and right margins and center) during late morning to early afternoon time periods. BOD bottles were kept in the dark in foil lined Styrofoam coolers in the

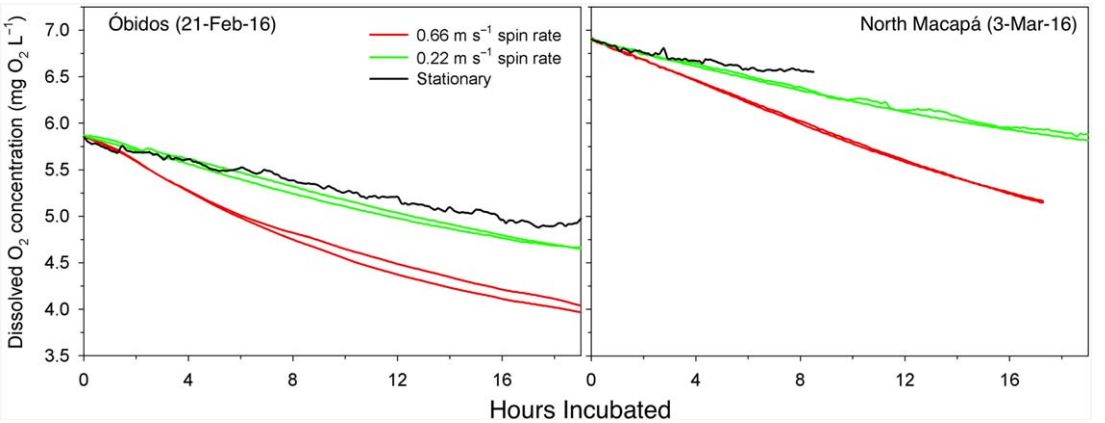

Fig. 2. Oxygen drawdown during incubations performed in the mainstem of the Amazon River at Óbidos (left) and near the river mouth (North Macapá; right) in a stationary incubation chamber (black) and two sets of duplicate chambers with spin rates of 20 rpm (green; 0.22 m s^{-1}) and 60 rpm (red; 0.66 m s^{-1}).

shade. BOD bottles were combusted before use and the chambers were acid-washed, rinsed with deionized water (DI) water, and sample rinsed.

Bacterial growth efficiency, or the amount of biomass produced relative to OM assimilated, ranges from below 0.05 to 0.6 in natural aquatic ecosystems (del Giorgio and Cole 1998), but rates reported for the Amazon River to date assume that all O_2 consumed is converted to CO_2. Previous experiments showed that 32.0% ± 7.6% and 46.4% ± 13.4% of ^{13}C-labeled vanillin and ^{13}C-labeled plant leachates were converted to CO_2 in the lower Amazon River mainstem and lowland tributaries, respectively (Ward et al. 2016). We used these values for calculation of the molar conversion of O_2 drawdown to CO_2 production under the assumption that the amount of labeled substrate not converted to CO_2 was assimilated as biomass or recycled.pCO_2 was measured during one of our discharge surveys across the mouth throughout a tidal cycle using a headspace equilibration chamber interfaced to a Licor 820 Infrared gas analyzer (Frankignoulle et al. 2001). River velocity, average depth, and discharge were measured across the channel at all sampling locations using a Sontek River Surveyor M9 Portable nine-beam 3.0 MHz/1.0 MHz/0.5 MHz ADCP. Cross-channel ADCP transects were performed at 1–2 h intervals for ~ 13 h in channels affected by tidal variation. CO_2 outgassing rates were measured using floating chambers as reported by Sawakuchi et al. (2017). Statistical significance was tested using unpaired *t*-tests with a 95% confidence interval.

Results and discussion

Linkage between river velocity and respiration

Evidence from rotating incubation experiments suggests that river respiration rates are dependent on the extent of particle suspension, which was controlled by rotation speed in the case of our experiments. In situ particle suspension is achieved when current velocity is equal to or greater than a particle's settling velocity in still water (Rubey 1933). In all experiments performed there was a linear drawdown of O_2 in the chambers, which was more temporally variable in the stationary chamber, and the rate of drawdown was positively correlated to the spin rate (r^2 = 0.76–1.00; Fig. 2; Supporting Information Table S1). Average respiration rates across all sites measured in the chambers rotated at 0.66 m s^{-1} (R_{3x}) and chambers rotated at 0.22 m s^{-1} (R_{1x}) were 2.4 and 1.4 times faster than in the stationary chambers (R_{STAT}) (Table 1).

We hypothesize that this relationship between rotational velocity and respiration rates exists because of the importance of interactions between suspended particles, dissolved constituents, and free-living and particle-bound microbes in driving aquatic metabolism. Particles are important receptors for microbial exoenzymes (Catalán et al. 2015) that enable processes such as priming effects to work effectively in aquatic environments (Ward et al. 2016). Further, the microbes associated with particles are significantly more metabolically active than free-living microbes along the lower Amazon River (Satinsky et al. 2015). The physiology and biological oxygen demand of *Escherichia coli* cells are directly dependent on small scale fluid motion, whereas stagnant fluids result in low activity (Coleman et al. 2003; Al-Homoud et al. 2007).

Bottle effects are another issue leading to underestimations of respiration rates determined by 60 mL BOD incubations (R_{BOD}). R_{BOD} was 2.7, 3.7, and 6.5 times slower than R_{STAT}, R_{1x}, and R_{3x}, respectively (Table 1). Although there is no direct evidence, this difference could perhaps be due to the development of anoxic micro-environments surrounding settled particles that limit microbial activity as opposed to a larger matrix volume with more heterogeneous conditions even when held stationary. Similar observations have been made with respect to primary production measurements in the ocean. For example, primary production rates were an

order of magnitude higher in 4 L compared to 30 mL bottles, which was attributed to enhanced algal mortality and a shift in the balance between production and carbon consumption (Gieskes et al. 1979).

The critical methodological issues resulting in respiration rate underestimations have been described above. The next challenge, which our experiments cannot fully address, is how to estimate actual in situ respiration rates based on the river velocity, especially considering the wide range of velocities observed along the lower river throughout seasons, tidal cycles, and within tributaries. For example, river velocity integrated across the channel and with depth ranged from 0.03 m s^{-1} at low water in the Xingu River to 1.76 m s^{-1} at Óbidos (Table 1). Velocity was highest at Óbidos, decreasing from an average of 1.36 ± 0.41 m s^{-1} to 0.64 ± 0.09 m s^{-1} across the mouth. An approach would be to normalize respiration rates in our chambers to in situ velocities using the observed linear correlation between chamber rotation velocity and respiration rates. However, this is not a straightforward calculation considering we do not fully understand how the fluid dynamics (and associated particle motion) within our chambers relate to turbulence and flow structure in the river itself. While ADCP measurements can begin to reconcile flow velocity structure, there is currently no robust theoretical basis for describing turbulent mixing in nature, and we rely on semi-empirical lab investigations (Gualtieri 2010). Given these logistical realities, our key point is that the main factor likely driving our observations of rotation-dependent respiration rates is that the particles in the fluid are in motion and suspended, regardless of how the motions are generated.

For a rough evaluation of whether flow is laminar or turbulent in our chambers and the river, which results in particle motion and mixing, we did a calculation of Reynold's numbers (Re) based on equations in the literature for rotational Re for the chambers and straight-flowing, uniformly round channel Re for the river, each factoring for velocity (rotational velocity in the case of chambers), radius of the system, kinematic viscosity, and water density (Reynolds 1883; Holman 2002; Childs 2010). Rotational Re within our chambers ranged from 1.4×10^4 to 4.2×10^4. Considering turbulent flow in rotating cylinders begins at Re values from 40 to 60 (Childs 2010), our chambers experienced turbulent flow at all rotation rates, and increasing the rotational velocity resulted in an equivalent increase in the dominance of inertial vs. viscous forces, inducing greater mixing at higher Re values as observed in other types of rotating cylinders (Sanders et al. 1981; Reich and Beer 1989; Bluemink et al. 2005).

Re ranged from 1.1×10^6 for the Tapajós River during low discharge to 2.7×10^8 at Óbidos during high discharge (Table 1). These Re values are well above the critical Re value for transition from laminar to turbulent flow in a straight flowing pipe (Re = 1000–2000) (Reynolds 1883; Holman 2002). While we did not evaluate in situ mixing rates, the extent to which river water and its dissolved and particulate load mixes is known to be directly linked to Re and the associated velocity and channel geometry (Bouchez et al. 2009; Gualtieri 2010; Potter et al. 2016). Further work is needed to quantify the relationship between river turbulence, velocity, and respiration to constrain spatiotemporal dynamics across the hydrodynamically complex lower river.

Carbon dioxide and river velocity linkages

Considering that dissolved CO_2 isotopic signatures in the lowland regions of the Amazon basin show little carbonate weathering-derived CO_2 entering from the surrounding landscape into the lower river, the concentration of dissolved CO_2 in the lower Amazon River mainstem is a dynamic balance between inputs from respiration of allochthonous and autochthonous OM (Mayorga et al. 2005), floodplains (Melack et al. 2009; Abril et al. 2014), and sediments (Devol et al. 1987) and outputs from gas evasion (Richey et al. 2002; Sawakuchi et al. 2017) and in situ primary production (Engle et al. 2008; Silva et al. 2009; Gagne-Maynard et al. 2017). CO_2 concentrations were lowest in the tributaries, with an average of 1470 ± 967 ppm compared to 3111 ± 1487 ppm in the upstream lower Amazon River mainstem sites (i.e., from Óbidos to Almeirim) and 2247 ± 1006 ppm across the mouth (Fig. 3).

pCO_2 in the mainstem consistently decreased downstream of Óbidos during each hydrologic period indicating that CO_2 losses occur more rapidly than the inputs along the lower river. River velocities also decreased downstream of Óbidos as the river channel(s) widen and disperse the river's discharge over a larger area (Table 1). An additional effect of the width and orientation of the lower Amazon River is increased gas transfer velocities due to a longer fetch and higher winds compared to further upstream, which maintains high outgassing rates even as pCO_2 decreases (Sawakuchi et al. 2017). Although it could be coincidental, a positive linear relationship was observed between pCO_2 and river velocity during each sampling period (Fig. 3A). Although there is no direct evidence, it is possible that the downstream decrease in pCO_2 is a result of decreasing respiration rates as the river slows down and outgassing rates remains high.

Similar observations were made during a series of transects performed throughout a tidal cycle across the river mouth (Fig. 3B). pCO_2 had a distinct cross channel pattern, with higher pCO_2 observed in a deep trough with faster water movement near the right margin (Fig. 3C). The magnitude of the maximum and minimum values observed across the river profile during each transect was linked to river velocity. The highest CO_2 concentrations were observed during ebb tide, reaching a maximum of 1642 ppm (Fig. 3). The right margin pCO_2 peak was 29% lower during the slowest river velocity transect (1174 ppm). Likewise, the minimum

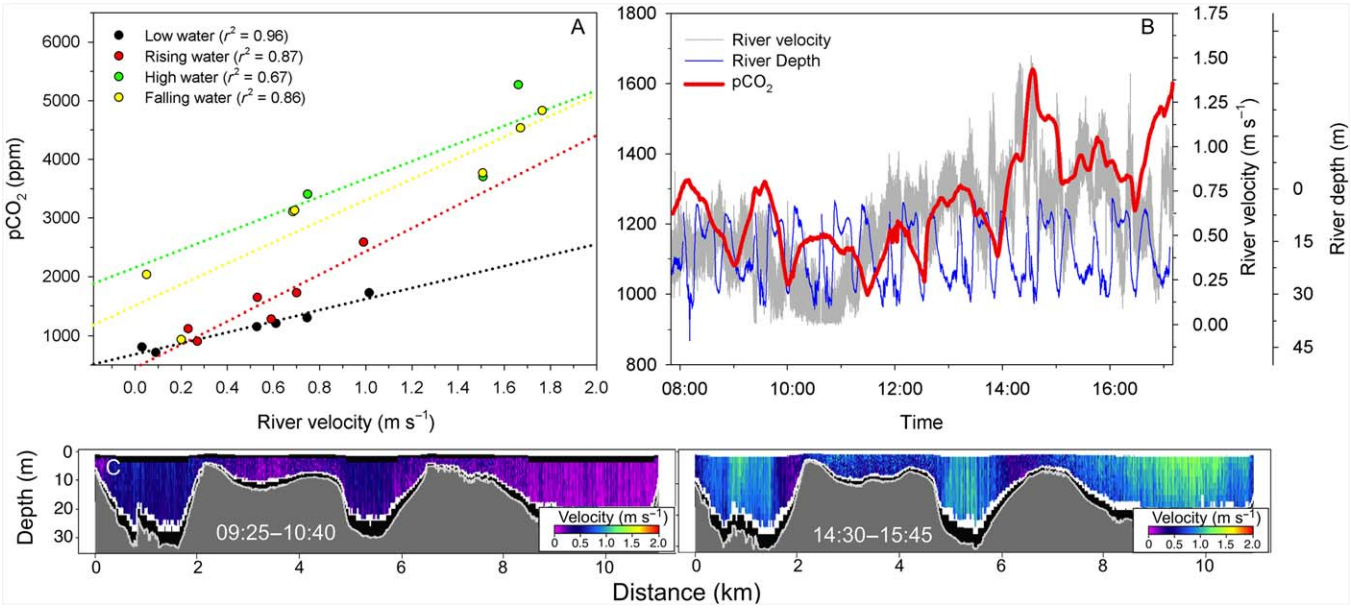

Fig. 3. Measurements of the partial pressure of dissolved CO_2 in the Amazon River mainstem at Óbidos, Almeirim, and the north/south channels across the river mouth near Macapá relative to average river velocity across each channel during low, rising, high, and falling water (**A**) and continuous measurements of the partial pressure of CO_2 and river velocity over a 12 h period in the north channel of Macapá during rising water (02 March 2016) (**B**). The river was crossed roughly once per hour during these transects to capture discharge throughout an entire tidal cycle. Velocity profiles are shown for the transects with minimum (-0.24 m s^{-1}) and maximum (0.80 m s^{-1}) average velocities (**C**).

pCO_2 observed during these two transects was 24% lower for the same low velocity transect (995 ppm) relative to the high velocity transect (1314 ppm). The average river velocity was 0.80 m s^{-1} and -0.24 m s^{-1} (e.g., negative value indicates river was flowing in reverse) during the maximum and minimum velocity transects, respectively, with the velocity being ~ 70% lower for the low velocity transect. For comparison, R_{1x} was 52% lower than R_{3x} during the same rising period in the North Channel of Macapá as a result of a 67% decrease in rotation velocity (Table 1).

The consistent variability in pCO_2 throughout the tidal cycle is compelling evidence for the reliance of CO_2 production rates on river velocity over short time scales that should be further examined. Outgassing rates should also theoretically be greatest during periods of high river velocity when surface conditions are more turbulent and gas transfer velocities are greater (Raymond and Cole 2001; Alin et al. 2011). Likewise, enzyme kinetics likely play an important role in shaping this hydrodynamic-biological linkage, but it is unclear how these kinetics respond within the chambers vs. in situ.

Contributions of respiration to river channel CO_2 outgassing

The amount of CO_2 produced by depth-integrated respiration was calculated across each channel using average depths measured during ADCP transects (Fig. 1; Table 1). R_{BOD} accounted for 12% ± 7% of average CO_2 outgassing rates in the lower Amazon River mainstem, from Óbidos to Macapá, and 58% ± 54% of CO_2 outgassing rates in the clearwater tributaries similar to past studies (Ellis et al. 2012). R_{1x} and R_{3x} accounted for 64% ± 22% and 104% ± 36%, of CO_2 outgassing rates, respectively, in the lower Amazon River mainstem and mouth sites compared to 295% ± 127% and 528% ± 428%, respectively, for the clearwater tributaries (Fig. 1). R_{3x} respiration rates essentially balanced CO_2 outgassing rates measured in the mainstem and mouth sites, which is, perhaps, not surprising considering the average mainstem river velocity (0.98 ± 0.42 m s^{-1}) was comparable to the 0.67 m s^{-1} rotation rate (bearing in mind the fluid dynamics caveats previously described). Although it is often assumed that primary production is minimal in the turbid mainstem, evidence from dissolved oxygen isotopes suggests that primary production occurs at roughly 25–50% the rate of respiration both upstream (Quay et al. 1995) and within our study domain (Gagne-Maynard et al. 2017). If these inferred photosynthetic rates are accurate, this could suggest that actual in situ respiration rates are higher than our R_{3x} rates due to higher river velocities than experienced in our chambers. Likewise, our floating chamber estimates of CO_2 outgassing do not capture all effects of the complex hydrodynamics on gas transfer.

Seasonally, respiration rates in the Amazon River mainstem were highest relative to CO_2 outgassing during rising water (Table 1). For example, during rising water, R_{1x} accounted for 149% ± 57% of CO_2 outgassing rates on average at the upstream Amazon River sites compared to 46% ± 15% at high water, 96% ± 91% during falling water, and 64% ± 15% at low water. The abundance of reactive OM during rising water in the

Amazon River (Ward et al. 2013, 2015, 2016) likely drives rates of respiration that exceed CO_2 outgassing as observed here, resulting in an accumulation of CO_2 in the water column. CO_2 concentrations peak at high water (Fig. 3) and begin to decline as CO_2 is outgassed more rapidly than respiration produces CO_2.

There has been a fundamental gap in our ability to quantify the processes that drive aquatic CO_2 production in large tropical rivers due to methodological bias. Here, we demonstrate that river velocity and hydrodynamic conditions are key physical factors controlling microbial metabolism of river-borne OM that has not been appropriately considered either conceptually or quantitatively. We have demonstrated that microbial respiration can potentially exceed CO_2 outgassing rates in the Amazon River mainstem and be balanced by primary production, outgassing, and other inputs. The apparent linkage between river velocity and respiration may have considerable implications when considering the impact of human activities that alter river flow such as damming and leveeing (Maavara et al. 2017). For example, alterations to inland water residence times by future impoundments and changes to the hydrologic cycle are expected to reduce the overall efficiency of OM breakdown in inland waters (Catalán et al. 2016). It remains unclear how this hydrodynamic-biogeochemical linkage will alter spatial distributions of carbon and energy balances along the land to sea continuum and higher trophic levels.

References

Abril, G., and others. 2014. Amazon River carbon dioxide outgassing fuelled by wetlands. Nature **505**: 395–398. doi:10.1038/nature12797

Al-Homoud, A., M. Hondzo, and T. LaPara. 2007. Fluid dynamics impact on bacterial physiology: Biochemical oxygen demand. J. Environ. Eng. **133**: 226–236. doi:10.1061/(ASCE)0733-9372(2007)133:2(226)

Alin, S. R., M.D.F.L. Rasera, C. I. Salimon, J. E. Richey, G. W. Holtgrieve, A. V. Krusche, and A. Snidvongs. 2011. Physical controls on carbon dioxide transfer velocity and flux in low-gradient river systems and implications for regional carbon budgets. J. Geophys. Res. Biogeosci. **116**: G01009. doi:10.1029/2010JG001398

Aufdenkampe, A. K., E. Mayorga, P. A. Raymond, J. M. Melack, S. C. Doney, S. R. Alin, R. E. Aalto, and K. Yoo. 2011. Riverine coupling of biogeochemical cycles between land, oceans, and atmosphere. Front. Ecol. Environ. **9**: 53–60. doi:10.1890/100014

Benner, R., S. Opsahl, G. Chin-Leo, J. E. Richey, and B. R. Forsberg. 1995. Bacterial carbon metabolism in the Amazon River system. Limnol. Oceanogr. **40**: 1262–1270. doi:10.4319/lo.1995.40.7.1262

Bluemink, J. J., E. A. Van Nierop, S. Luther, N. G. Deen, J. Magnaudet, A. Prosperetti, and D. Lohse. 2005. Asymmetry-induced particle drift in a rotating flow. Phys. Fluids **17**: 72106. doi:10.1063/1.1978921

Bouchez, J., E. Lajeunesse, J. Gaillardet, C. France-Lanord, P. Dutra-Maia, and L. Maurice. 2009. Turbulent mixing in the Amazon River: The isotopic memory of confluences. Earth Planet. Sci. Lett. **290**: 37–43. doi:10.1016/j.epsl.2009.11.054

Catalán, N., A. M. Kellerman, H. Peter, F. Carmona, and L. J. Tranvik. 2015. Absence of a priming effect on dissolved organic carbon degradation in lake water. Limnol. Oceanogr. **60**: 159–168. doi:10.1002/lno.10016

Catalán, N., R. Marcé, D. N. Kothawala, and L. J. Tranvik. 2016. Organic carbon decomposition rates controlled by water retention time across inland waters. Nat. Geosci. **9**: 501–504. doi:10.1038/ngeo2720

Childs, P. R. 2010. Rotating flow. Elsevier.

Cole, J. J., D. L. Bade, D. Bastviken, M. L. Pace, and M. Van de Bogert. 2010. Multiple approaches to estimating air-water gas exchange in small lakes. Limnol. Oceanogr.: Methods **8**: 285–293. doi:10.4319/lom.2010.8.285

Coleman, M. E., M. L. Tamplin, J. G. Phillips, and B. S. Marmer. 2003. Influence of agitation, inoculum density, pH, and strain on the growth parameters of *Escherichia coli* O157: H7—relevance to risk assessment. Int. J. Food Microbiol. **83**: 147–160. doi:10.1016/S0168-1605(02)00367-7

del Giorgio, P., and P. M. Williams [eds.]. 2005. Respiration in aquatic ecosystems. Oxford Univ. Press.

del Giorgio, P. A., and J. J. Cole. 1998. Bacterial growth efficiency in natural aquatic systems. Annu. Rev. Ecol. Syst. **29**: 503–541. doi:10.1146/annurev.ecolsys.29.1.503

Devol, A. H., P. D. Quay, and J. E. Richey. 1987. The role of gas exchange in the inorganic carbon, oxygen, and ^{222}Rn budgets of the Amazon River. Limnol. Oceanogr. **32**: 235–248. doi:10.4319/lo.1987.32.1.0235

Ellis, E. E., J. E. Richey, A. K. Aufdenkampe, A. V. Krusche, P. D. Quay, C. Salimon, and H. Brandão da Cunha. 2012. Factors controlling water-column respiration in rivers of the central and southwestern Amazon Basin. Limnol. Oceanogr. **57**: 527–540. doi:10.4319/lo.2012.57.2.0527

Engle, D. L., J. M. Melack, R. D. Doyle, and T. R. Fisher. 2008. High rates of net primary production and turnover of floating grasses on the Amazon floodplain: Implications for aquatic respiration and regional CO_2 flux. Glob. Chang. Biol. **14**: 369–381. doi:10.1111/j.1365-2486.2007.01481.x

Filizola, N., and J. L. Guyot. 2004. The use of Doppler technology for suspended sediment discharge determination in the River Amazon. Hydrol. Sci. J. **49**: 143–153. doi:10.1623/hysj.49.1.143.53990

Frankignoulle, M., A. Borges, and R. Biondo. 2001. A new design of equilibrator to monitor carbon dioxide in highly dynamic and turbid environments. Water Res. **35**: 1344–1347. doi:10.1016/S0043-1354(00)00369-9

Gagne-Maynard, W. C., and others. 2017. Evaluation of primary production in the lower Amazon River based on a

dissolved oxygen stable isotopic mass balance. Front. Mar. Sci. **4**: 1–12. doi:10.3389/fmars.2017.00026

Gålfalk, M., D. Bastviken, S. Fredriksson, and L. Arneborg. 2013. Determination of the piston velocity for water-air interfaces using flux chambers, acoustic Doppler velocimetry, and IR imaging of the water surface. J. Geophys. Res. Biogeosci. **118**: 770–782. doi:10.1002/jgrg.20064

Gieskes, W. W. C., G. W. Kraay, and M. A. Baars. 1979. Current ^{14}C methods for measuring primary production: Gross underestimates in oceanic waters. Neth. J. Sea Res. **13**: 58–78. doi:10.1016/0077-7579(79)90033-4

Gualtieri, C. 2010. RANS-based simulation of transverse turbulent mixing in a 2D geometry. Environ. Fluid Mech. **10**: 137–156. doi:10.1007/s10652-009-9119-6

Hess, L. L., J. M. Melack, A. G. Affonso, C. Barbosa, M. Gastil-Buhl, and E. M. Novo. 2015. Wetlands of the lowland Amazon basin: Extent, vegetative cover, and dual-season inundated area as mapped with JERS-1 synthetic aperture radar. Wetlands **35**: 745–756. doi:10.1007/s13157-015-0666-y

Holman, J. P. 2002. Heat transfer. McGraw Hill.

Hotchkiss, E. R., and R. O. Hall, Jr. 2014. High rates of daytime respiration in three streams: Use of $\delta^{18}O_{O2}$ and O_2 to model diel ecosystem metabolism. Limnol. Oceanogr. **59**: 798–810. doi:10.4319/lo.2014.59.3.0798

Hotchkiss, E. R., R. O. Hall, Jr, R. A. Sponseller, D. Butman, J. Klaminder, H. Laudon, M. Rosvall, and J. Karlsson. 2015. Sources of and processes controlling CO_2 emissions change with the size of streams and rivers. Nat. Geosci. **8**: 696–699. doi:10.1038/ngeo2507

Ivanova, A. A., V. G. Kozlov, and A. V. Chigrakov. 2004. Dynamics of a fluid in a rotating horizontal cylinder. Fluid Dyn. **39**: 594–604. doi:10.1023/B:FLUI.0000045675.82694.6c

Johnson, M. S., J. Lehmann, S. J. Riha, A. V. Krusche, J. E. Richey, J. P. H. Ometto, and E. G. Couto. 2008. CO_2 efflux from Amazonian headwater streams represents a significant fate for deep soil respiration. Geophys. Res. Lett. **35**: L17401. doi:10.1029/2008GL034619

Kremer, J. N., S. W. Nixon, B. Buckley, and P. Roques. 2003. Conditions for using the floating chamber method to estimate air-water gas exchange. Estuaries Coast. **26**: 985–990. doi:10.1007/BF02803357

Lorke, A., and others. 2015. Drifting versus anchored flux chambers for measuring greenhouse gas emissions from running waters. Biogeosci. Discuss. **12**: 14619–14645. doi:10.5194/bg-12-7013-2015

Maavara, T., R. Lauerwald, P. Regnier, and P. Van Cappellen. 2017. Global perturbation of organic carbon cycling by river damming. Nat. Commun. **8**: 15347. doi:10.1038/ncomms15347

Marcarelli, A. M., C. V. Baxter, M. M. Mineau, and R. O. Hall. 2011. Quantity and quality: Unifying food web and ecosystem perspectives on the role of resource subsidies in freshwaters. Ecology **92**: 1215–1225. doi:10.1890/10-2240.1

Matthews, C. J., V. L. St. Louis, and R. H. Hesslein. 2003. Comparison of three techniques used to measure diffusive gas exchange from sheltered aquatic surfaces. Environ. Sci. Technol. **37**: 772–780. doi:10.1021/es0205838

Mayorga, E., A. K. Aufdenkampe, C. A. Masiello, A. V. Krusche, J. I. Hedges, P. D. Quay, J. E. Richey, and T. A. Brown. 2005. Young organic matter as a source of carbon dioxide outgassing from Amazonian rivers. Nature **436**: 538–541. doi:10.1038/nature03880

McClain, M. E., and others. 2003. Biogeochemical hot spots and hot moments at the interface of terrestrial and aquatic ecosystems. Ecosystems **6**: 301–312. doi:10.1007/s10021-003-0161-9

Melack, J. M. 2016. Aquatic ecosystems, p. 119–148. In L. Nagy, B. R. Forsberg, and P. Artaxo [eds.], Interactions between biosphere, atmosphere and human land use in the Amazon basin. Springer.

Melack, J. M., E.M.L.M. Novo, B. R. Forsberg, M. T. F. Piedade, and L. Maurice. 2009. Floodplain ecosystem processes, p. 525–541. *In* J. Gash, M. Keller, and P. Silva-Dias [eds.], Amazonia and global change. American Geophysical Union.

Moreira-Turcq, P., P. Seyler, J. L. Guyot, and H. Etcheber. 2003. Exportation of organic carbon from the Amazon River and its main tributaries. Hydrol. Process. **17**: 1329–1344. doi:10.1002/hyp.1287

Potter, M. C., D. C. Wiggert, and B. H. Ramadan. 2016. Mechanics of fluids, 5th ed. Nelson Education.

Quay, P. D., J. E. Richey, A. H. Devol, R. Benner, and B. R. Forsberg. 1995. The ^{18}O:^{16}O of dissolved oxygen in rivers and lakes in the Amazon basin: Determining the ratio of respiration to photosynthesis rates in freshwaters. Limnol. Oceanogr. **40**: 718–729.

Raymond, P. A., and J. J. Cole. 2001. Gas exchange in rivers and estuaries: Choosing a gas transfer velocity. Estuaries Coast. **24**: 312–317. doi:10.2307/1352954

Raymond, P. A., and others. 2013. Global carbon dioxide emissions from inland waters. Nature **503**: 355–359. doi:10.1038/nature12760

Reich, G., and H. Beer. 1989. Fluid flow and heat transfer in an axially rotating pipe—I. Effect of rotation on turbulent pipe flow. Int. J. Heat Mass Transf. **32**: 551–562. doi:10.1016/0017-9310(89)90143-9

Reynolds, O. 1883. An experimental investigation of the circumstances which determine whether the motion of water shall be direct or sinuous, and of the law of resistance in parallel channels. Proc. R. Soc. Lond. **35**: 84–99. doi:10.1098/rspl.1883.0018

Richey, J. E., J. M. Melack, A. K. Aufdenkampe, V. M. Ballester, and L. L. Hess. 2002. Outgassing from Amazonian rivers and wetlands as a large tropical source of atmospheric CO_2. Nature **416**: 617–620. doi:10.1038/416617a

Rubey, W. W. 1933. Settling velocity of gravel, sand, and silt particles. Am. J. Sci. **148**: 325–338. doi:10.2475/ajs.s5-25.148.325

Sanders, J., D. D. Joseph, and G. S. Beavers. 1981. Rimming flow of a viscoelastic liquid inside a rotating horizontal cylinder. J. Nonnewton Fluid Mech. **9**: 269–300. doi:10.1016/0377-0257(81)85005-7

Satinsky, B. M., and others. 2015. Metagenomic and metatranscriptomic inventories of the lower Amazon River, May 2011. Microbiome **3**: 39. doi:10.1186/s40168-015-0099-0

Sawakuchi, H. O., and others. 2017. Carbon dioxide emissions along the lower Amazon River. Front. Mar. Sci. **4**. doi:10.3389/fmars.2017.00076

Silva, T. S. F., M. P. F. Costa, and J. M. Melack. 2009. Annual net primary production of macrophytes in the eastern Amazon floodplain. Wetlands **29**: 747–758. doi:10.1672/08-107.1

Tranvik, L. J., and others. 2009. Lakes and reservoirs as regulators of carbon cycling and climate. Limnol. Oceanogr. **54**: 2298–2314. doi:10.4319/lo.2009.54.6_part_2.2298

Ward, N. D., and others. 2013. Degradation of terrestrially derived macromolecules in the Amazon River. Nat. Geosci. **6**: 530–533. doi:10.1038/ngeo1817

Ward, N. D., and others. 2015. The compositional evolution of dissolved and particulate organic matter along the lower Amazon River-Óbidos to the ocean. Mar. Chem. **177**: 244–256. doi:10.1016/j.marchem.2015.06.013

Ward, N. D., and others. 2016. The reactivity of plant-derived organic matter and the potential importance of priming effects along the lower Amazon River. J. Geophys. Res. Biogeosci. **121**: 1522–1539. doi:10.1002/2016JG003342

Ward, N. D., T. S. Bianchi, P. M. Medeiros, M. Seidel, J. E. Richey, R. G. Keil, and H. O. Sawakuchi. 2017. Where carbon goes when water flows: Carbon cycling across the aquatic continuum. Front. Mar. Sci. **4**. doi:10.3389/fmars.2017.00007

Wissmar, R. C., J. E. Richey, R. F. Stallard, and J. M. Edmond. 1981. Plankton metabolism and carbon processes in the Amazon River, its tributaries, and flooplain waters, Peru-Brazil, May-June 1977. Ecology **62**: 1622–1633. doi:10.2307/1941517

Acknowledgments

Funding was provided by NSF DEB Grant 1256724, FAPESP Grant 08/58089-9, and the University of Florida Jon L. and Beverly A. Thompson Endowment. Preparation of supplies was performed by Rebekka Gould and Jaqui Neibauer at the University of Washington. Field logistics were assisted by Daimio Brito, Rodrigo da Silva, and Troy Beldini. Laboratory and field assistance were provided by William Gagne-Maynard and Joel Melo-Diniz. Research was performed aboard the Barco de Pesquisa "Mirage."

Submitted 14 March 2017
Revised 30 June 2017; 12 October 2017; 17 December 2017
Accepted 20 December 2017